Reduction of Propionic Acid over a Pd-Promoted ReO_x/SiO_2 Catalyst Probed by X-Ray Absorption Spectroscopy and Transient Kinetic Analysis

James D. Kammert[a], Jiahan Xie[a], Ian J. Godfrey[b], Raymond R. Unocic[c], Eli Stavitski[d], Klaus Attenkofer[d], Gopinathan Sankar[b] Robert J. Davis[a,]*

a) University of Virginia Department of Chemical Engineering, 102 Engineer's Way, PO Box 400741, Charlottesville, VA 22904-4741, United States

b) University College London Department of Chemistry, 20 Gordon St, Bloomsbury, London WC1H 0AJ, United Kingdom

c) Center for Nanophase Materials Sciences, Oak Ridge National Laboratory, 1 Bethel Valley Road, Oak Ridge, TN, 37831, United States

d) National Synchrotron Light Source II, Building 740, Brookhaven National Lab, Upton, NY 11973, United States

ABSTRACT

A Pd-promoted Re/SiO_2 catalyst was prepared by sequential impregnation and compared to monometallic Pd/SiO_2 and Re/SiO_2. All samples were characterized by electron microscopy, H_2 and CO chemisorption, H_2 temperature-programmed reduction, and *in-situ* X-ray absorption spectroscopy at the Re L_{III} and Pd K-edges. The samples were also tested in the reduction of propionic acid to 1-propanol and propionaldehyde at 433 K in 0.1-0.2 MPa H_2. Whereas monometallic Pd was inactive for carboxylic acid reduction, monometallic Re catalyzed aldehyde formation, but only after high-temperature pre-reduction that produced metallic Re. When Pd was present with Re in a bimetallic catalyst, Pd facilitated the reduction of Re in H_2 to ~4+ oxidation state at modest temperatures, producing an active catalyst for the conversion of propionic acid to 1-propanol. Under the conditions of this study, the orders of reaction in propionic acid and H_2 were approximately zero and one, respectively. Transient kinetic analysis of the carboxylic acid reduction to alcohols revealed that at least 50% of the Re in the bimetallic catalyst participated in the catalytic reaction. The Pd is proposed to enhance the catalytic activity of the bimetallic catalyst by spilling over hydrogen that can partially reduce Re and react with surface intermediates.

KEYWORDS: Carboxylic acid; propionic acid; 1-propanol; propionaldehyde; rhenium; palladium; X-ray absorption spectroscopy; transient kinetics

INTRODUCTION

The recent increase in demand for renewable chemical feedstocks and carbon-neutral sources of energy has placed the spotlight on the utilization of biomass and bio-oil for the production of chemicals and fuels.[1–4] Specialty chemicals are still produced mostly by the transformation of fossil fuels[5] as they offer better returns on investment due to decades of research and development. In contrast to the functionalization chemistry required to convert oil derivatives into consumer products, biomass conversion will require the development of defunctionalization processes.[6]

One area of focus in biomass conversion research is the utilization of lauric oils, e.g. coconut and palm kernel oils, containing significant amounts of short- and medium-chain fatty acids.[7] The free fatty acids and triglycerides in these feedstocks have carbon chain lengths between C_6 and C_{22}, which can be refined to fatty alcohols for use as detergents, lubricants, plasticizers, and high-performance oils for jet engines[4,7] via reduction of the acid functional group. The development of low-cost processes for the production of these types of specialty chemicals has the potential to increase the sustainability and CO_2-neutrality of the chemicals and fuels industries.[2,8]

The current industrial process to produce renewable fatty alcohols involves the reduction of fatty acid esters over a copper-based catalyst.[4,7,9–11] Traditionally, the catalyst used in the process is copper chromite ($CuCr_2O_4$), also known as an Adkins-type catalyst, which consists of a mixed oxide of copper and chromium. It can be extruded with clay or other supports, and is mixed with alkali or alkaline earth metals to improve its activity.[10,11] While copper chromite has been known to be an effective catalyst for many years, recent concerns about the leaching of toxic Cr^{6+} ions[9,12,13] have prompted research on non-chromium-containing catalysts. Additionally, the conditions used to carry out this process commercially are known to be rather extreme, utilizing H_2 pressures

upwards of 25 MPa.[9] Therefore, the design of a catalyst that can operate under lower pressure conditions is highly desirable.

The bulk fermentation of sugars by engineered micro-organisms has the potential to selectively produce a variety of carboxylic acids on a large scale.[14,15] Short-chain carboxylic acids can also be produced by the fast pyrolysis of biomass, where potential applications of this bio-oil will require remediation of the resulting acidity.[16] Direct reduction of carboxylic acids (instead of esters) to alcohols is thus a motivation of research on new catalysts, in order to take advantage of this large-scale production of free acids. Recent work has shown the reduction of carboxylic acids can be catalyzed by a variety of metal and metal oxide surfaces, generally consisting of a mixture of reducible precious metal and oxophilic metal components. Examples include studies by Primo et al.[17] and Rachmady and Vannice[18] who demonstrated the activity of Ru and Pt supported on TiO_2. Catalysts such as $RuSn/Al_2O_3$[19] and $RuMo/ZrO_2$[20] have also been studied for reduction of carboxylic acids in polar solvents. More detailed information about the reduction of carboxylic acids and their derivatives can be found in the review by Pritchard et al.[21]

Rhenium in particular has demonstrated an ability to catalyze the selective reduction of carboxylic acids to alcohols. More than a half century ago, solid rhenium oxide surfaces having Re in several different oxidation states were active in the reduction of a number of carboxylic acids at 423-443 K and dihydrogen pressures between 13.5 and 27.0 MPa.[22–25] In most cases, the major product was the corresponding monoalcohol, with yields reported up to 100%. The patent literature reports on several inventions describing the use of supported rhenium catalysts promoted by palladium, silver, and copper.[26–29] A recent study by Takeda et al. involving Ru, Rh, Ir, Pt, and Pd added to a Re/SiO_2 catalyst reported that the Pd-promoted Re/SiO_2 system is the most active and selective of these materials for the reduction of stearic acid in a 1,4-dioxane solvent[30], and that the

metal-promoted Re catalysts are capable of operating at significantly lower H_2 pressures and temperatures than those required by Re alone.

The support of the Pd-promoted Re-based (PdRe) catalysts has a significant influence on their activity in the liquid-phase reduction of fatty acids to fatty alcohols. Takeda et al. demonstrated that PdRe was significantly more active on a SiO_2 support than on a variety of other supports including Al_2O_3, TiO_2, and C, and that Re was the main active material in the catalyst.[30] Corbel-Demailly et al. reported that PdRe/TiO_2 catalyzed the aqueous-phase reduction of succinic and levulinic acids to their corresponding α,ω-diols.[31] Interestingly, Rozmyslowicz et al. demonstrated that a monometallic Re/TiO_2 catalyst could still facilitate the reduction of stearic acid in decane solvent without Pd promotion after pretreatment with H_2 at 673 K.[32] The underlying reasons for the observed influence of the support and promoter remain unclear. Besson et al. used X-ray photoelectron spectroscopy (XPS) to conclude that active catalysts for reduction of succinic and levulinic acids to their corresponding diols in the aqueous phase appeared to consist mostly of Re oxide in a 3+ oxidation state.[31,33–36] Both Re/SiO_2 and PdRe/SiO_2 catalysts were characterized after catalytic reduction of stearic acid in dioxane using *ex-situ* X-ray absorption spectroscopy (XAS).[37] White line analysis of the Re L_{III} edge data suggested that Re in these materials resides in an average oxidation state near 2+ after reaction, which has also been reported to be among the active oxidation states of Re as a bulk oxide.[23]

To remove the complicating influence of solvents and liquid phase acids, we have studied the catalyst structure and transient reaction kinetics of carboxylic acid reduction in the gas phase. The investigation of a Pd-promoted Re/SiO_2 catalyst under gas phase reduction conditions should eliminate the dissolution of metals that can also cause particle growth. In particular, *in-situ* X-ray absorption spectroscopy and *ex-situ* electron microscopy were used to examine the chemical state

and distribution of the metal components on the catalyst support and the transient kinetic analysis provided important information on the utilization of Re in the active material, which is currently unknown.

EXPERIMENTAL METHODS

Catalyst synthesis

Catalysts used in this study were synthesized by an incipient wetness impregnation method, with each component of the catalyst being added stepwise as outlined by Takeda et al.[30] For example, the desired loading of the metal salt (aqueous tetraaminepalladium(II) nitrate, 10 wt%, Aldrich; ammonium perrhenate, Aldrich, 99%) was added to a quantity of distilled, deionized water (16.8 MΩ) to form a solution equal in volume to the pore volume of the SiO_2 support (Fuji Silysia Chemical Ltd, 0.72 $cm^3\ g^{-1}$, 511 $m^2\ g^{-1}$). This solution was mixed with the support until a homogeneously-distributed sample was formed. The impregnated sample was dried at 368 K in air for 12 h, and then treated in air at 773 K for 3 h after ramping for 3 h. In the bimetallic catalyst, the Re was added first, prior to heating in air to 773 K, after which the Pd solution was added to the supported Re catalyst, dried in air at 368 K, and heated in air to 773 K for a second time. The weight loading of supported metals after synthesis was determined by inductively coupled plasma optical emission spectroscopy (ICP-OES) performed by Galbraith Laboratories, Knoxville, TN.

Adsorption of H_2, CO, and N_2

The chemisorption of H_2 (Praxair, 5.0) and CO (Praxair, 3.0) and physisorption of N_2 (Praxair, 5.0) were carried out using a Micromeritics ASAP 2020 instrument. Prior to chemisorption measurements, samples were heated to 473 K (Pd/SiO_2, $PdRe/SiO_2$) or 673 K (Re/SiO_2) under flowing H_2 at 4 K min^{-1}, then held at 473 K (or 673 K) for 1 hour under flowing H_2. The samples were then evacuated at 473 K and degassed for 2 h before cooling to 373 K or

308 K for H_2 chemisorption or 308 K for CO chemisorption. Either H_2 or CO was dosed from 0.001-0.06 MPa, and the total monolayer chemisorption values are reported after extrapolation of the higher pressure linear region of the isotherm to zero pressure. Prior to N_2 physisorption measurements, catalysts were degassed by heating to 723 K under vacuum for 4 h before cooling to liquid N_2 temperature for analysis. Physisorption results were analyzed using the BET analysis of the N_2 (Praxair, 5.0) adsorption isotherm.

Temperature-Programmed Reduction

Temperature-programmed reduction (TPR) was carried out using a Micromeritics AutoChem II 2920 instrument equipped with a thermal conductivity detector. All catalysts were heated to 308 K under Ar (Praxair, 5.0) before switching to a reducing gas mixture. The reducing gas mixture of 5% H_2 in Ar (Praxair, certified mixture) passed through the catalyst bed at a flow rate of 50 cm^3 min^{-1} while the bed temperature was ramped at 10 K min^{-1} to 573 K.

Transmission Electron Microscopy

Transmission electron microscopy (TEM), scanning transmission electron microscopy with a high-angle annular dark-field detector (STEM-HAADF) and energy-dispersive X-ray spectroscopy (EDS) were performed on an FEI Titan 80-300 operating at 300 kV that is equipped with a Gatan 794 Multi-scan Camera (EFTEM) and an energy-dispersive spectrometer for elemental X-ray analysis at the University of Virginia. High-resolution STEM-HAADF imaging with EDS mapping was carried out using a Hitachi HF-3300 operating at 300 kV and equipped with a Bruker SDD-EDS detector at Oak Ridge National Lab. Samples were prepared by sonicating 50 mg of each sample in cyclohexane or hexanes for 30 min, followed by dropwise impregnation onto a Ni or Au grid coated with lacey carbon (400 mesh, Ted Pella).

X-ray Absorption Spectroscopy

In-situ X-ray absorption spectroscopy (XAS) was carried out on beamline B18 of the Diamond Light Source (DLS) at the Harwell Science & Innovation Campus, Didcot, United Kingdom, operated at 3.0 GeV and with a typical current of *ca.* 300 mA. The setup of this beamline has been described previously.[38] All XAS measurements associated with Re were performed in transmission at the Re L_{III}-edge (10.535 keV). The XAS measurements associated with Pd were performed in fluorescence using a 9 element Ge solid state detector at the Pd K-edge (24.353 keV). Both edges were collected with a spot size of 0.2 x 0.25 mm. The Re L_{III}-edge experiments performed at DLS used a Si(111) double crystal monochromator and Cr-coated harmonic rejection mirrors. Experiments performed at the Pd K-edge used a Si(311) double crystal monochromator with Pt-coated harmonic rejection mirrors. The XAS experiment relevant to the high-temperature reduction of Re/SiO_2 was carried out on beamline 8-ID of the National Synchrotron Light Source II (NSLS-II) at Brookhaven National Laboratory in Brookhaven, New York, operated at 3.0 GeV and with a typical current of *ca.* 325 mA. The capabilities of this beamline have previously been summarized.[39] The Re L_{III}-edge experiments performed at NSLS-II used a Si(111) double crystal monochromator with uncoated Si higher harmonic rejection mirrors and a spot size of 0.25 mm.

To secure samples in the beam path, pellets of catalyst were pressed gently to form flat cylinders, and the amount of catalyst for transmission experiments was adjusted to give an edge jump ($\triangle\mu x$) of around 1. At DLS, these pellets were placed inside an *in-situ* reaction chamber made of bored-through poly-ether ether ketone (PEEK). Kapton windows were secured in place with poly(trifluoroethylene) washers on either side of the chamber to ensure a gas-tight seal. The PEEK reaction chamber was held in place by a bronze sample holder with a heating element so that the temperature of the reaction chamber could be controlled. A Re foil (Goodfellow, 12.5 μm,

99.99%) was used as a reference at the Re L_{III}-edge, and a Pd metal foil (Goodfellow, 12.5 μm, 99.95%) was used as a reference at the Pd K-edge. For the high-temperature pretreatment, a brass sample holder was used in place of the PEEK chamber.

Before each treatment, the fresh catalyst pellet was first purged of O_2 by flushing the reaction chamber for 15 min with N_2. To perform the *in-situ* experiments, two different methods were used. In the first method, designated as "no pretreatment" or NP, 4% H_2 in N_2 was passed through a room-temperature saturator containing propionic acid and then over the catalyst at 30 cm^3 min^{-1} for 15 min before ramping the temperature at 3 K min^{-1} to 413 K. The temperature was held at 413 K for 1 h before ramping again at 3 K min^{-1} to 433 K. The temperature was then held at 433 K for 1 h after which the sample was cooled to room temperature and purged with pure N_2. In the second method, designated as "low-temperature pretreatment" or LTP, 4% H_2 in N_2 was passed over the catalyst for 15 min at 30 cm^3 min^{-1} before ramping the temperature at 3 K min^{-1} to 453 K. The temperature was held at 453 K for 30 min before cooling at 10 K min^{-1} to 433 K when the flow was passed through a saturator containing propionic acid and then over the catalyst bed. The temperature was then held at 433 K for 1 h then cooled at 10 K min^{-1} to 413 K and held for 1 h after which the sample was cooled to room temperature and purged with pure N_2. The "high-temperature pretreatment", abbreviated HTP, was performed by first purging the sample chamber with N_2 at 100 cm^3 min^{-1}. The gas flow was then switched to 4% H_2 in N_2 and the catalyst bed was then heated to 673 K at 6 K min^{-1}. The catalyst bed was held at 673 K for 1 h, and then cooled to 433 K. The catalyst bed was held at 433 K for 20 minutes while spectra were collected and then cooled to room temperature.

All XAS results were processed using Demeter XAS analysis freeware created by Bruce Ravel.[40] Results from X-ray absorption near-edge spectroscopy (XANES) were background-

corrected and normalized uniformly at each edge using Athena, an XAS background correction application that is part of the Demeter software package. The oxidation state of each sample was determined by the shift in the maximum of the derivative in the edge energy compared to known standards.[41,42] The standards used for Re were Re metal foil, (Goodfellow, 12.5 μm, 99.99%), ReO_2 powder (Aldrich, 99.7%), ReO_3 powder (Pfaltz & Bauer, 99.9%) and Re_2O_7 powder (Aldrich 99.9%) for oxidation states of 0, +4, +6, and +7, respectively. The standards used for Pd were Pd foil (Goodfellow, 12.5 μm, 99.95%), and PdO powder (Aldrich, 99.999%), for oxidation states of 0 and +2, respectively. The EXAFS results were also background corrected and normalized in Athena, then k^3-weighted and Fourier transformed to change from k-space to R-space. The R-space data for standards were then fitted to multi-shell models over k-ranges from approximately 3 to 13 for Pd and 3 to 16 for Re at nodes in the fine structure. Fitting was performed in Artemis with FEFF6, yielding an S_0^2 value of 0.830 for all metallic Re shells, 0.748 for all oxidized Re shells, 0.829 for all metallic Pd shells, and 0.641 for all oxidized Pd shells.

Reduction Reactions

The reduction of propionic acid (Sigma Aldrich, 99.5%) to 1-propanol and propionaldehyde or butyric acid (Sigma-Aldrich, 99.0%) to 1-butanol and butyraldehyde was carried out in a stainless steel downward flow reactor with inner diameter 0.46 cm contained within the reactor system depicted in Figure 1. The catalyst bed consisted of the supported metal catalyst powder (0.060-0.140 g) resting on a plug of glass wool. Temperature measurements were made using a thermocouple inserted from the top of the reactor tube into the middle of the catalyst bed. Prior to reaction, the system (including the liquid saturators) was purged with flowing N_2 at 30 cm^3 min^{-1} for at least 10 min. After purging with N_2, the reactor was purged with H_2 at 15 cm^3 min^{-1} for 10 min before ramping the temperature to 433 K. Once the temperature was stable the

flow was passed through a stainless-steel saturator to form a mixture of 1 vol.% carboxylic acid in H_2 (0.1-0.22 MPa) that was fed to the catalyst bed. The effluent gases were separated and quantified using an SRI 8610C gas chromatograph (GC-FID) equipped with an MXT-WAX column (0.53 mm i.d., 30 m) and a flame-ionization detector (FID). To obtain order of reaction in H_2, the H_2 partial pressure was varied by partially replacing H_2 with N_2 at the appropriate flowrate while maintaining a constant pressure of acid. To obtain the order of reaction in acid, the partial pressure of the acid was varied while maintaining a constant pressure of H_2. The total flowrate was kept constant for all variations in reactant partial pressures.

The conversion of the acid to its corresponding aldehyde and alcohol was evaluated from the integrated product peak areas. Methane was used as the internal standard, which prevented the quantification of any C_2 through C_4 hydrocarbons that might have been formed during the kinetic experiments. Hydrocarbon products were typically produced in very low amounts (between 5-10% selectivity) under the conditions studied here. The fractional conversion (f_i) of acid i to its corresponding alcohol and aldehyde products j was calculated using the expression

$$f_i = \frac{\sum M_j}{M_i + \sum M_j} \tag{1}$$

where M_j is the molar flow rate of the component j. Similarly, the selectivity of the reaction towards each product j was calculated using the expression

$$S = \frac{M_j}{\sum M_j} \tag{2}$$

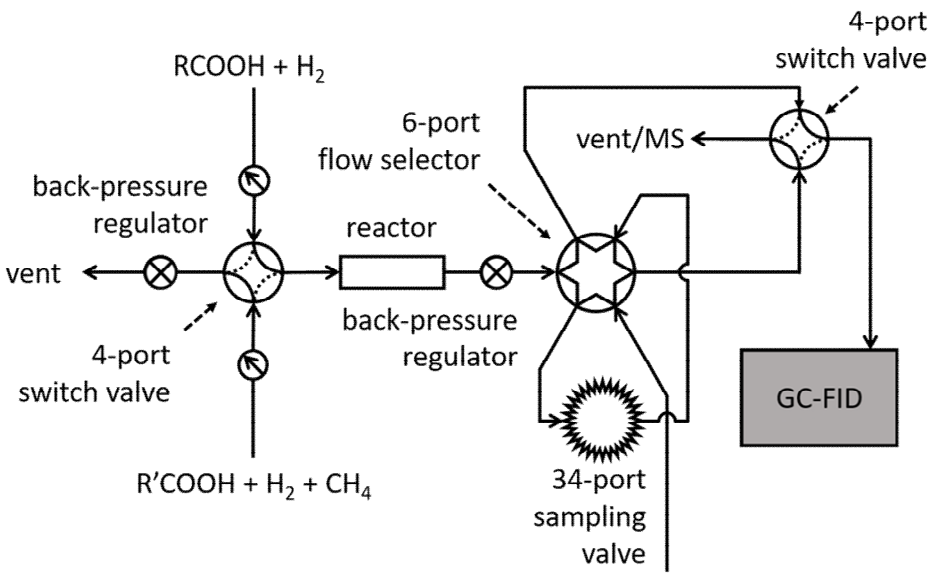

Figure 1: **Schematic representation of the reactor system used to collect steady-state and transient reaction kinetics.**

Transient Kinetic Analysis

The transient kinetic analysis carried out in this work was performed in a manner analogous to steady-state isotopic transient kinetic analysis (SSITKA).[43] This technique can be used to approximate the turnover frequency and number of reactive intermediates leading to products on the active sites of a catalyst. The SSITKA technique is a well-established method that has been used by our group to investigate ammonia synthesis[44,45], CO oxidation[46,47], CO hydrogenation[48], and the Guerbet coupling of ethanol.[49,50] All transient kinetic experiments performed in the current study were carried out using the reactor that is illustrated in Figure 1.

The transient kinetic experiment proceeds by first allowing a reaction to reach steady-state, and then abruptly switching from the reactant to a different (but structurally similar) reactant that is converted at a similar rate (in this case modified only by the insertion of a CH_2 group into the carbon chain) and observing the transient response of the system. In the experiments reported here,

the transient response of the catalyst after switching between butyric and propionic acid was studied. In a typical switching experiment, an inert tracer is fed with one of the reactant streams to correct for the gas-phase holdup in the reactor system. Figure 2 presents an ideal normalized transient kinetic response curve after replacing butyric acid with propionic acid. The decay of the tracer is indicative of the characteristic gas-phase holdup of the reactor system, representative of the non-ideal nature of the step switch assuming there is no interaction between the inert tracer and the catalyst surface. After the switch in reactant acid from C_4 to C_3, the products of these acids will decrease (C_4) or increase (C_3), crossing near 0.5, as shown in Figure 2.

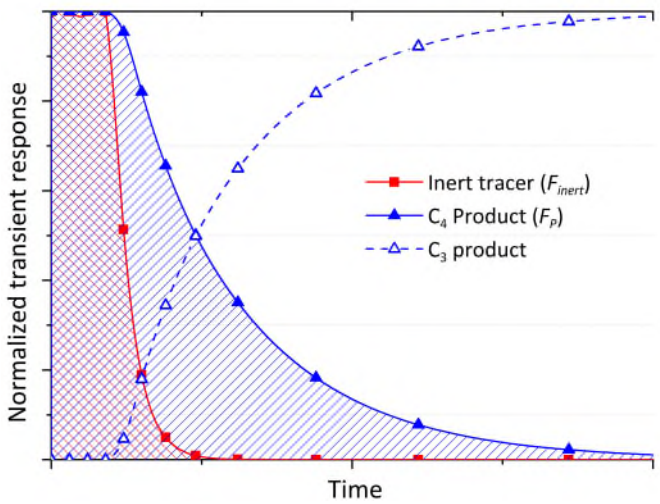

Figure 2: **Theoretical transient response curves for products undergoing a reactant switch from C_4 reactant to C_3 reactant. Decay of the inert tracer (red squares) is used to correct for the gas-phase holdup of the reactor system when calculating the mean surface residence time from the integral of the C_4 product decay (filled blue triangles) and C_3 product replacement (open blue triangles).**

As is commonly done in the SSITKA experiment, kinetic parameters can be derived from the individual normalized transient response curves (F_i). The area below each normalized transient response curve is representative of the mean surface residence time (τ_i) after correction by the response of the inert tracer, given by

$$\tau_i = \int_{t_0}^{\infty} (F_i - F_{inert}) dt \tag{3}$$

Here the inverse of the mean surface residence time is equivalent the turnover frequency of the catalyst for the given product, or simply

$$TOF_i = (\tau_i)^{-1} \tag{4}$$

From the mean surface residence time τ_i and the rate of formation of a product by the catalyst (R_i), it is also possible to calculate the surface coverage of reactive intermediates (N_i) leading to a given product, given by

$$N_i = R_i \cdot \tau_i \tag{5}$$

Further discussion of the SSITKA technique and considerations can be found in the review by Shannon and Goodwin.[43]

The SSITKA method works well because there is almost no perturbation in the steady state rate during the switch between different isotopes of the reactant. In the transient method used in this work, we switched between C_4 and C_3 acids to acquire the transient kinetics. There was a small difference in the steady state rate of conversion of these two acids, but the difference did not appear to significantly affect the expected transient behavior as summarized in Figure 2. The transient kinetic experiments performed in this work were carried out using the reaction procedure described

in Section 0. The reaction was allowed to come to steady-state during conversion of the original reactant, at which point flow was started through the modified reactant saturator. Once the flow had stabilized, the reactant flow path was switched from the original reactant saturator to the modified reactant saturator using a 4-way valve. The transient behavior of the product alcohols was monitored with time on stream using the GC-FID described earlier, while the transient behavior associated with the aldehyde was monitored by collecting samples of the reactor effluent in the 34-port sampling valve with 16 samples loops depicted in Figure 1 and subsequently injecting the samples into the GC-FID. The influence of flow rate was explored by simply adjusting the gas flows and repeating the experiment.

RESULTS

Elemental Analysis and Adsorption of H_2, CO, and N_2

Results from ICP-OES, H_2 and CO chemisorption, and N_2 physisorption for the catalysts studied in this work are shown in Table 1. Each of the catalysts had a high surface area, greater than 400 $m^2\ g^{-1}$, which is similar to the support. The elemental analysis for the Re loading revealed about 1.0-1.5 wt% less Re than the nominal loading, which may be the result of partial volatilization of Re_2O_7 during the 773 K thermal treatments.

The chemisorption of H_2 on the monometallic Pd catalyst at 373 K indicates approximately 39% of Pd atoms were exposed, assuming a stoichiometry of H to surface Pd equal to 1. When the temperature of the H_2 chemisorption was decreased to 308 K, chemisorption increased by 50%, consistent with the formation of a β-PdH phase. During chemisorption of CO, a stoichiometry of between 0.5 and 1 for CO/Pd is appropriate.[51] Assuming a CO to surface Pd ratio of 0.75[52], the fraction of Pd exposed is equal to 43%, which is consistent with the results from H_2 chemisorption.

In contrast, the monometallic Re catalyst and the PdRe bimetallic catalyst chemisorbed a smaller fraction of H_2 at 373 K, with a H/metal ratio of 0.11 for both samples. This low uptake was likely a result of the high barrier to H_2 chemisorption on Re.[53] The total uptake of H_2 on the PdRe catalyst at 373 K was below the additive total of 37.1 μmol g_{cat}^{-1} that would be expected if each metal (Pd, Re) adsorbed independently and was of the same dispersion as their monometallic counterparts. The higher total uptake of H_2 on the PdRe catalyst at 308 K compared to that at 373 K is consistent with the formation of a β-PdH phase, as observed with the monometallic Pd catalyst. This result can be compared to previously reported H_2 uptake results on a Pd-promoted Re/Al_2O_3 catalyst[54] that showed strong interaction of Pd with Re, which inhibited the formation of bulk β-PdH. Even in the presence of excess Re, apparently minimal interaction between the Re and Pd left the surface Pd on our $PdRe/SiO_2$ catalyst available for reaction with H_2 leading to formation of bulk β-PdH. Results from CO chemisorption on the Re-containing catalysts also revealed relatively low uptake, with a CO/Re ratio of 0.16 for the monometallic catalyst and a CO/metal ratio of 0.13 for the bimetallic catalyst. Similar to the case with H_2, the uptake of CO was below the additive total of 88.2 μmol g_{cat}^{-1} that would be expected from independent adsorption onto a mixture the two metals that was equally as dispersed as their monometallic counterparts. These chemisorption results indicate a change in dispersion or metal availability in at least one of the supported metal components when the two metals are combined on one support.

For the PdRe catalyst, surface Pd still accounts for some of the observed H_2 chemisorption, resulting in the increase in H_2 uptake relative to either of the monometallic catalysts. In the case of CO chemisorption, a different trend is observed. The CO chemisorption uptake on the $PdRe/SiO_2$ is nearly identical to that measured on the Re/SiO_2. Previous work has shown that Re^{7+} and Re^{4+} interact weakly with CO leading to minimal chemisorption[55], while completely reduced

Re demonstrates higher CO chemisorption uptake.[56] The observation that CO chemisorption on the PdRe catalyst was not a simple combination of adsorption on Pd/SiO_2 and Re/SiO_2 is attributed to a larger fraction of partially-oxidized Re species present in the bimetallic system, which had undergone a lower temperature H_2 pretreatment than the more highly reduced Re/SiO_2 after high temperature reduction.

Table 1: **Results from elemental analysis and gas adsorption.**

Sample	Metal loading (wt %)		Surface Area (m^2 g^{-1})	Chemisorption (μmol g_{cat}^{-1})		
				H_2 (373 K)	H_2 (308 K)	CO (308 K)
Pd/SiO_2	1.03% Pd	--	484	18.9	30.9	31.7
Re/SiO_2	--	6.52% Re	433	19.8	17.6	57.7
$PdRe/SiO_2$	0.88% Pd	6.91% Re	460	24.9	32.4	60.0

Temperature Programmed Reduction

As illustrated in Figure 3, the monometallic Pd catalyst began to reduce immediately upon heating H_2, with maximum hydrogen consumption rate at 354 K. The monometallic Re catalyst did not consume any H_2 until 525 K and reached a maximum consumption rate at 536 K. The bimetallic catalyst exhibited two H_2 consumption peaks at low temperature, with maxima at 353 K and 368 K, and no H_2 consumption peaks at higher temperatures. These results agree with those from H_2 TPR reported previously using a number of reducible, noble-metal-promoted, oxophilic metal oxides supported on SiO_2,[30] and on Pd-promoted Re supported on Al_2O_3 systems.[57] The TPR results in Figure 3 suggest that the addition of Pd to a Re catalyst lowers the temperature at which the Re is reduced, presumably by spillover of atomic H from Pd to the Re. In addition, low-melting-temperature metal oxides, such as Re_2O_7 with a melting point of 630 K, are capable of spreading across oxide supports and reacting during thermal treatments due to their low Tammann

temperatures.[58] The mobility of Re^{7+} oxides could have resulted in the migration of Re toward Pd during heating, leading to lower temperature reduction via spillover of surface H from Pd to Re.

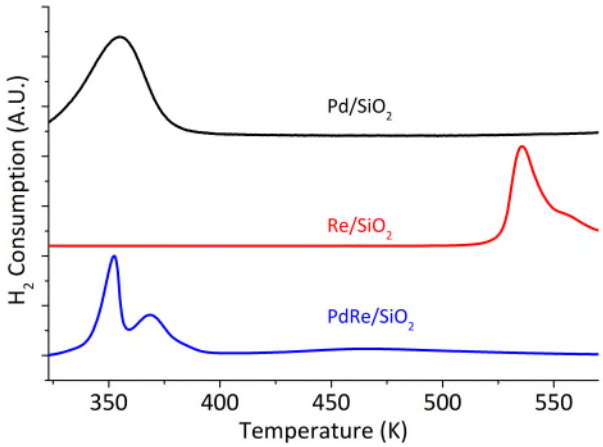

Figure 3: **Temperature programmed reduction of the synthesized catalysts at a ramp rate of 10 K min^{-1}.**

Transmission Electron Microscopy

Image analysis of the fresh $PdRe/SiO_2$ catalyst acquired by STEM-HAADF shown in Figure 4 gave an average metal particle size of 3.2±1.5 nm. Elemental analysis by EDS (shown in Figure S1) showed the fresh catalyst particles had many smaller particles that contained only Re and fewer larger particles containing Pd. The average metal particle size of $PdRe/SiO_2$ after use in propionic acid reduction increased slightly to 3.9±1.5 nm. The mapping of the metallic components of the $PdRe/SiO_2$ catalyst after use in propionic acid reduction is shown in Figure 5. The mapping results revealed that Pd and Re were not co-located. Whereas Pd EDS mapping correlates well with the visible nanoparticles in Figure 5a, the Re EDS mapping suggests Re is highly dispersed across the surface of the material.

Image analysis of the fresh and used Pd/SiO_2 catalysts by STEM HAADF gave an average particle size of 3.1±0.8 nm and 3.0±1.0 nm, respectively. Image analysis of the fresh Re/SiO_2 was

consistent with a very wide range of particles. Some Re particles were >100 nm whereas Re was also detected by EDS on SiO_2 regions in which no particles could be imaged. Evidently much of the Re is highly dispersed across much of the support. After use for 24 h in the reduction of 1 kPa propionic acid in 0.1 MPa H_2 at 433 K, the Re was observed to transform into to a mixture of larger particles ~20-50 nm across and highly dispersed particles of an average size <1 nm. Images of the monometallic catalysts can be found in the supporting information in Figures S2 and S3.

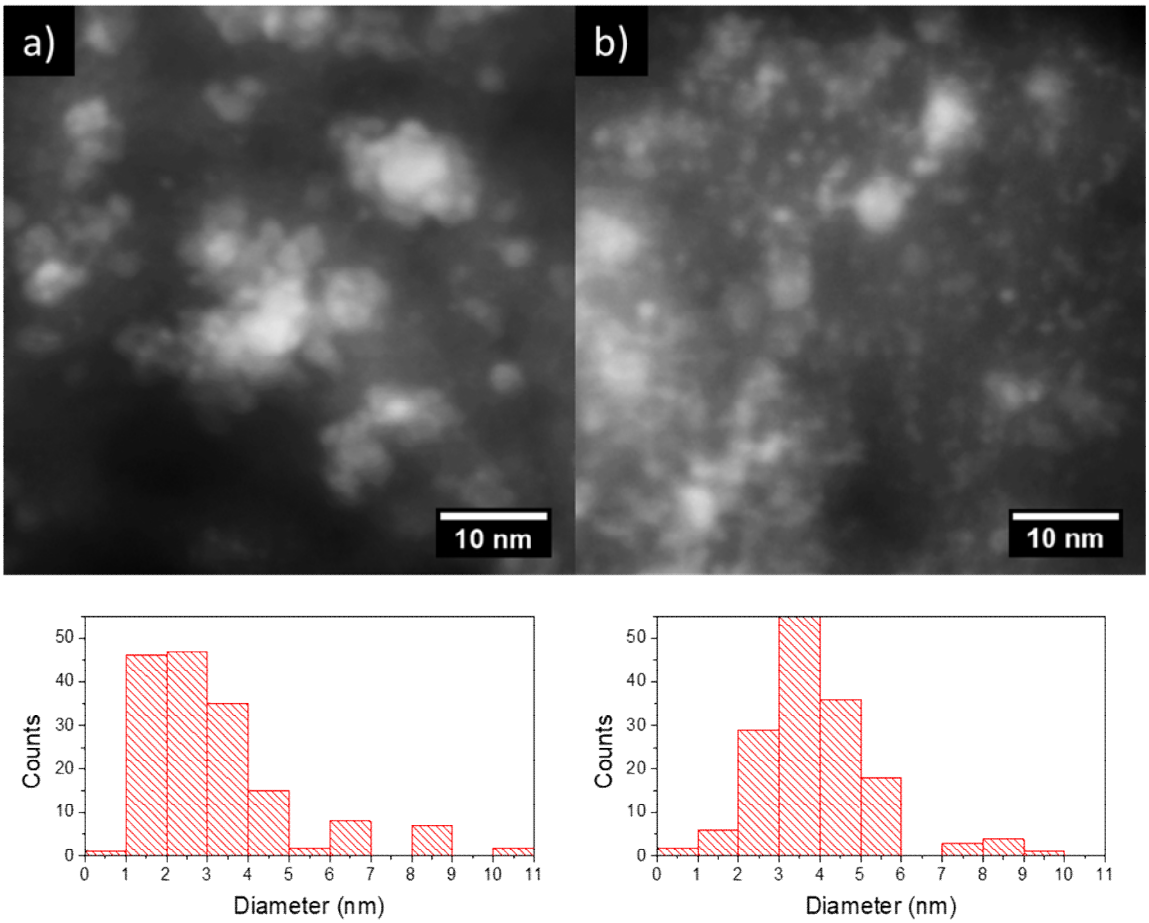

Figure 4: **STEM-HAADF images of $PdRe/SiO_2$ catalyst (a) before and (b) after use for the reduction of propionic acid for 24 h with associated particle size distributions. Reactions were carried out at 433 K, in 0.1 MPa H_2 and 1 kPa propionic acid.**

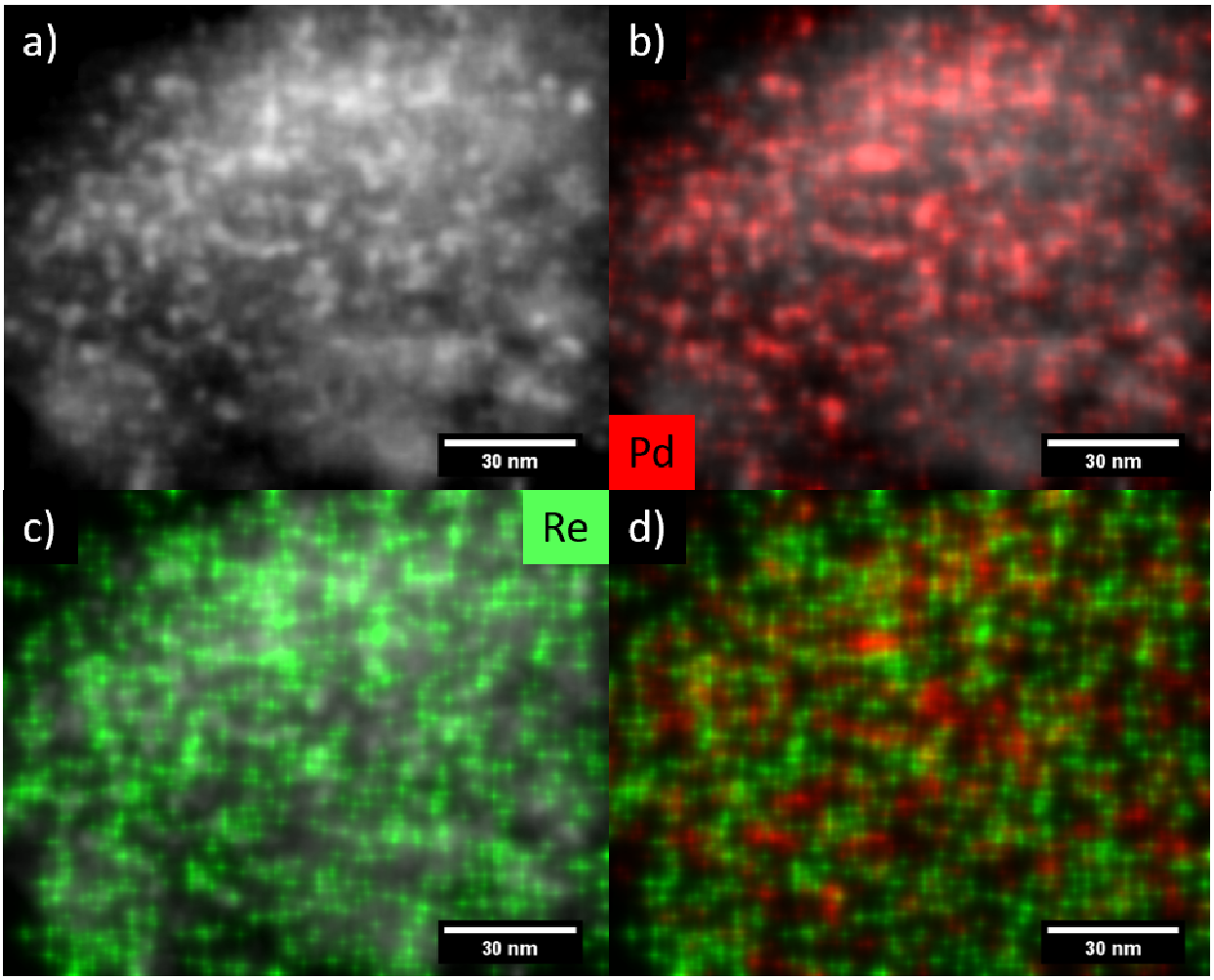

Figure 5: **STEM-EDS mapping of PdRe/SiO_2 catalyst after reduction of 1 kPa propionic acid in 0.1 MPa H_2 for 24 h at 433 K, showing (a) STEM image, (b) EDS signal corresponding to Pd overlaid on STEM image, (c) EDS signal corresponding to Re overlaid on STEM image, and (d) composite EDS signals corresponding to Pd and Re.**

X-ray Absorption Spectroscopy

The Re L_{III}-edge XANES associated with the catalyst samples are shown in Figure 6. The highest whiteline intensity (maximum absorbance at the absorption edge) was associated with the as-synthesized catalysts at room temperature prior to exposure to H_2 or H_2/acid mixtures. The whiteline intensity and the edge position, defined as the first maximum of the first derivative of the absorption edge, were both consistent with Re in the air-exposed catalysts residing in a 7+ oxidation state, typical of Re_2O_7.

A correlation between the Re L_{III}-edge energy and the formal oxidation state of each Re standard was used to approximate the oxidation state of the catalysts in the presence of reactant gases. Previous studies have shown that the oxidation state and edge position of Re oxides at the L_{III}-edge appear fairly linear between Re^0 and Re^{6+}, while Re^{7+} does not follow the same linear trend.[41,42] In order to minimize the error of this correlation at higher oxidation states, a linear interpolation was used between each of the data points. The results of this correlation can be seen in Figure 6b and d. When the monometallic Re/SiO_2 catalyst was treated at low temperature (433-453 K) in flowing 4% H_2 in N_2, with or without co-fed propionic acid, the Re appeared to reduce slightly to an average oxidation state between Re^{6+} and Re^{7+} as can be seen in Figure 6d. At the higher pretreatment temperature of 673 K (HTP), the monometallic Re/SiO_2 was reduced in H_2 very nearly to metal, which is consistent with the TPR results showing this elevated temperature is required to substantially reduce the supported Re species.

The as-synthesized PdRe/SiO_2 catalyst at room temperature had spectral features associated with Re^{7+}, similar to the as-synthesized monometallic Re/SiO_2 catalyst. When the

$PdRe/SiO_2$ was directly exposed to propionic acid vapor in the 4% H_2/N_2 mixture at 433 K (NP) to simulate reaction conditions, the Re L_{III} edge whiteline intensity and the edge energy decreased, corresponding to an average oxidation state of +5.0. When the as-synthesized $PdRe/SiO_2$ catalyst was pretreated at 453 K (LTP) in flowing 4% H_2 in N_2, the Re L_{III} edge whiteline intensity decreased more significantly and the edge position moved to even lower energy, associated with reduction to an average oxidation state of +3.6. Evidently, the slightly higher pretreatment temperature in H_2 was able to more extensively reduce Re than the reaction conditions. Most importantly, the presence of Pd facilitated the low-temperature partial reduction of Re, consistent with results from H_2 TPR (Figure 3).

The EXAFS fitting results from the *in-situ* experiments are summarized in Table 2, and the fitting results for the standards are summarized in the supporting information in Table S1. As the ratio of tetrahedrally coordinated to octahedrally coordinated Re in Re_2O_7 may vary depending on the ratio of bulk to molecularly dispersed material[59], the first shell Re-O coordination number could not be used to make conclusions about the Re species present. Instead, analysis of the EXAFS corresponding to the Re oxide standards revealed that as the oxidation state of Re decreased, the Re-O interatomic distance increased, as shown in Figure S4. When the first shell Re-O scattering paths of the oxide standards were fitted, the average Re-O distance was observed to increase with decreasing oxidation state from 1.74 Å for Re-O in Re_2O_7 to 2.00 Å for Re-O in ReO_2. The EXAFS in Figure 7a did not reveal significant changes in the first-shell Re-O interatomic distance for Re/SiO_2 samples treated up to 453 K in H_2, with or without propionic acid. The EXAFS in Figure 7b associated with $PdRe/SiO_2$ showed a clear increase in the first-shell Re-O interatomic distance, indicating that the Re in the $PdRe/SiO_2$ catalysts was reduced significantly. The fitted Re-O bond distances of 2.033 (NP) and 2.072 Å (LTP) for the $PdRe/SiO_2$ catalysts under

4% H_2/N_2 and acid are slightly elongated from the ReO_2 standard. These elongated Re-O distances suggest that Re has an oxidation state between 3+ and 4+ in the $PdRe/SiO_2$ under reaction conditions. Representative EXAFS fitting results are shown in Figure S5.

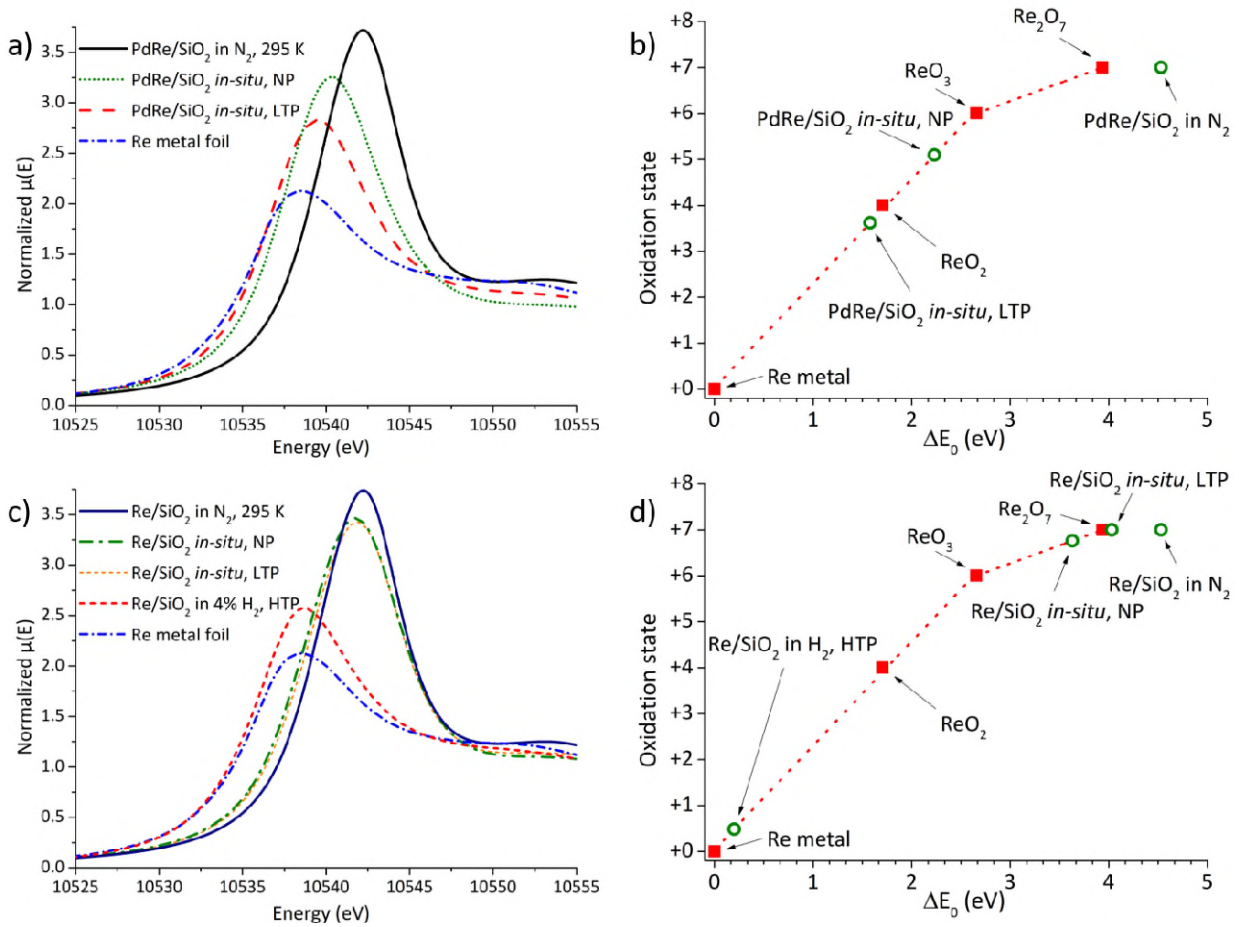

Figure 6: **Re L_{III} edge XANES and correlated average oxidation states. Spectra were collected at 433 K unless specified, and spectra denoted "*in-situ*" were collected in flowing 4% H_2/N_2 passing through a room temperature propionic acid saturator. (a) $PdRe/SiO_2$ XANES before treatment, and after NP or LTP. (b) Correlation between edge energy and oxidation state for $PdRe/SiO_2$. (c) Re/SiO_2 XANES before treatment, and after NP, LTP, or without propionic acid after HTP. (d) Correlation between edge energy and oxidation state for Re/SiO_2.**

The Pd K-edge XANES shown in Figure 8 and Figure S6 confirmed that Pd in both the bimetallic PdRe and monometallic Pd samples was oxidic after synthesis but was reduced to metal under reaction conditions. The Pd K-edge EXAFS were consistent with a first shell Pd-Pd coordination number of between 8.1 and 8.5 (depending on pretreatment) for Pd/SiO_2 under reaction conditions, correlating to about 70% dispersion assuming spherical metal particles[60],which is consistent with an average particle size of 1.5 nm. Although the Pd particle size estimated from EXAFS is slightly below that estimated from H_2 chemisorption and electron microscopy, all of the techniques suggest that Pd is highly dispersed on the catalyst surface. No Pd-Re interactions were evident based on the Pd K-edge EXAFS of either of the studied $PdRe/SiO_2$ samples (without pretreatment or pretreated at 453 K) under reaction conditions. Representative radial distribution functions of the Pd samples can be found in Figure S4 in the supporting information.

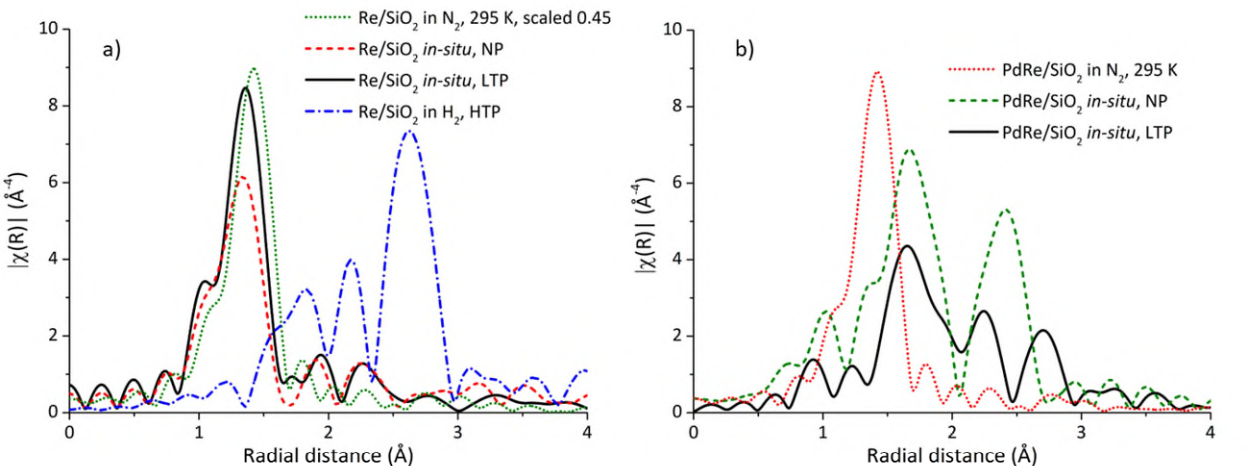

***Figure 7*: (a) Magnitude of the Fourier transform (not corrected for phase shift) of the Re L_{III}-edge EXAFS associated with (a) Re/SiO_2 and (b) $PdRe/SiO_2$ after various pretreatments. Spectra were collected at 433 K unless specified, and spectra denoted as "*in-situ*" were collected in flowing 4% H_2/N_2 passing through a room temperature propionic acid saturator.**

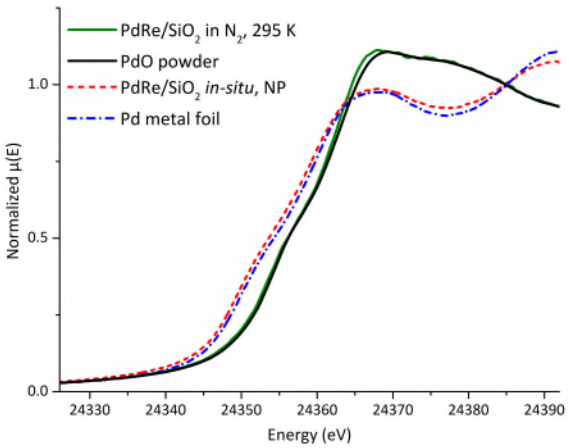

Figure 8: **Pd K-edge near-edge spectra. Solid lines are for as-synthesized $PdRe/SiO_2$ compared to PdO standard. Dashed lines are for the $PdRe/SiO_2$ sample under reaction conditions (433 K, in 4% H_2/N_2 passed through a room temperature propionic acid saturator) compared to Pd metal foil.**

Table 2: **EXAFS fitting results for SiO_2-supported PdRe, Re, and Pd catalysts.**

Sample	Pretreatment	*In-situ*	Temp. (K)	Edge	Shell	*R (Å)*	*N*	σ^2 *(Å^2)*	ΔE_0 *(eV)*	*R-factor*
$PdRe/SiO_2$	none	N_2	Ambient	Re L_{III}	Re-O	1.737 ±0.002	4.5 ±0.2	0.0010 ±0.0003	6.9 ±0.6	0.02
				Pd K	Pd-O	2.021 ±0.007	4.1 ±0.3	0.0006 ±0.0010		
				Pd K	Pd-Pd	3.059 ±0.013	4.7 ±2.0	0.0041 ±0.0030	-1.7 ±0.9	0.01
				Pd K	Pd-Pd	3.451 ±0.009	5.4 ±2.7	0.0039 ±0.0036		
	NP	4% H_2/N_2, propionic acid	433	Re L_{III}	Re-O	2.033 ±0.014	4.5 ±0.6	0.0051 ±0.0015	8.9 ±2.1	0.02
				Pd K	Pd-Pd	2.738 ±0.002	8.1 ±0.3	0.0078 ±0.0003	-5.5 ±0.3	0.01
	LTP	4% H_2/N_2, propionic acid	433	Re L_{III}	Re-O	2.079 ±0.021	2.6 ±0.5	0.0044 ±0.0027	9.7 ±2.3	0.03
				Pd K	Pd-Pd	2.739 ±0.003	8.2 ±0.4	0.0077 ±0.0004	-5.4 ±0.4	0.01
Re/SiO_2	none		Ambient	Re L_{III}	Re-O	1.737 ±0.007	4.5 ±0.5	0.0010 ±0.0007	7.0 ±1.7	0.01
	NP	4% H_2/N_2, propionic acid	433	Re L_{III}	Re-O	1.683 ±0.016	2.0 ±0.4	0.0023 ±0.0014	-10. ±4.7	0.03
	LTP		433	Re L_{III}	Re-O	1.691 ±0.010	2.0 ±0.3	0.0011 ±0.0010	-0.8 ±2.7	0.02
	HTP	4% H_2/N_2	433	Re L_{III}	Re-O	2.023 ±0.021	2.0 ±0.6	0.0098 ±0.0044	6.3 ±1.7	0.03
				Re L_{III}	Re-Re	2.759 ±0.008	5.7 ±0.6	0.0073 ±0.0007		
Pd/SiO_2	none	N_2	Ambient	Pd K	Pd-O	2.029 ±0.009	4.0 ±0.5	0.0011 ±0.0014		
				Pd K	Pd-Pd	3.061 ±0.021	4.1 ±2.8	0.0058 ±0.0051	-0.6 ±1.2	0.03
				Pd K	Pd-Pd	3.456 ±0.015	4.8 ±3.8	0.0055 ±0.0058		
	NP	4% H_2/N_2, propionic acid	433	Pd K	Pd-Pd	2.739 ±0.003	8.5 ±0.4	0.0088 ±0.0004	-5.3 ±0.3	0.01
	LTP		433	Pd K	Pd-Pd	2.750 ±0.004	8.2 ±0.4	0.0094 ±0.0005	-5.9 ±0.4	0.01

Catalytic Reduction of Propionic Acid

The rates of conversion of propionic acid to 1-propanol and propionaldehyde over $PdRe/SiO_2$ and Re/SiO_2 catalysts at steady state are summarized in Table 3. The Pd/SiO_2 sample is not shown in Table 3 as it only produced a small amount of light hydrocarbons. Over $PdRe/SiO_2$, 1-propanol was the major product of the reaction, but the selectivity shifted towards propionaldehyde at the highest flowrate (lowest conversion). Small amounts (5-10%) of light hydrocarbons were also observed in the product stream, but are not included in Table 3 because of overlap with the methane internal standard. Hydrocarbon products have previously been attributed to the decarbonylation or decarboxylation of the C_N acid to form C_{N-1} hydrocarbons or the secondary reduction of the C_N alcohol to form C_N hydrocarbons.[32] The increase in 1-propanol selectivity with increasing acid conversion suggests that most of the propionaldehyde was subsequently hydrogenated to 1-propanol on the catalyst. A physical mixture of the monometallic Re/SiO_2 and Pd/SiO_2 catalysts with the same ratio of metals was also tested for reduction of propionic acid. The relative rate over the physical mixture was only 30% of that of the bimetallic catalyst under the same conditions, but both systems produced a majority of alcohol product. When the H_2 pressure and propionic acid concentration were varied over $PdRe/SiO_2$, the alcohol formation reaction was observed to be first order and nearly zero order, respectively, as shown in Figure 9. These orders of reaction are similar to those that have been reported previously for stearic acid reduction in 1,4-dioxane[36] and for the reduction of octanoic acid in a decane solvent (see Figure S8), suggesting the reaction mechanism is unchanged by the presence of solvent**.**

The rate of propionic acid conversion over Re/SiO_2 pretreated at 673 K in H_2 was substantially lower than that measured over $PdRe/SiO_2$ (Table 3). The high temperature pretreatment of Re/SiO_2 was needed to reduce the supported Re oxide and generate catalytic

activity, which is consistent with the TPR results in Figure 3. Over Re/SiO_2, the major product of propionic acid reduction was propionaldehyde. Extrapolation of the results in Table 3 for Re/SiO_2 to infinite flowrate indicates an initial selectivity to propionaldehyde of 97%, suggesting that the primary reaction during propionic acid reduction over Re/SiO_2 is aldehyde formation. In all of the cases reported here, the linear dependence of propionic acid conversion on inverse flowrate indicates the reaction was differential as is illustrated in Figure S9.

Table 3: **Steady state reduction of propionic acid over $PdRe/SiO_2$ and Re/SiO_2 at 433 K, 1 kPa propionic acid in 0.1 MPa H_2.**

Catalyst	Gas flow rate (cm^3 min^{-1})	Conversion (%)	Rate of acid conversion (mol g_{cat}^{-1} h^{-1})	Selectivity of oxygenates[a]	
				1-propanol	propionaldehyde
$PdRe/SiO_2$	15	7.1	1.6×10^{-4}	80	20
	30	4.0	2.0×10^{-4}	74	26
	60	2.5	2.4×10^{-4}	64	36
Re/SiO_2[b]	18	4.3	6.3×10^{-5}	22	78
	28	2.2	4.2×10^{-5}	13	87
	51	1.4	4.8×10^{-5}	11	89

(a) Does not account for the small amount of light hydrocarbons
(b) Re/SiO_2 was pretreated at 673 K under flowing H_2 for 1 h

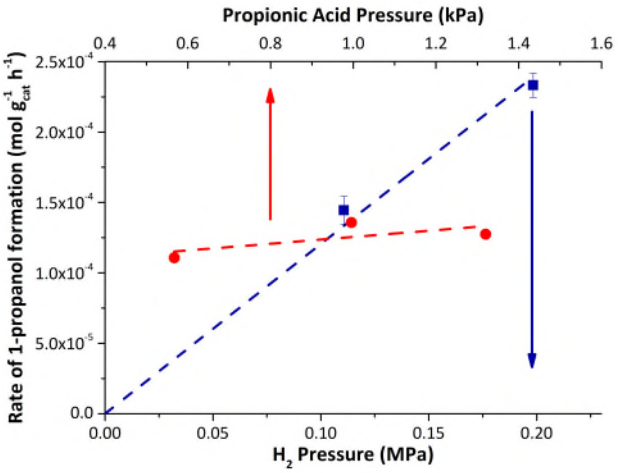

***Figure 9*: Influence of reactant partial pressures on observed rate of 1-propanol formation over PdRe/SiO_2 at 433 K. When H_2 pressure was varied, propionic acid pressure was held at 1 kPa, and when propionic acid pressure was varied, H_2 pressure was held at 0.1 MPa.**

Transient Kinetic Analysis of Carboxylic Acid Reduction

The mean surface residence times of species leading to alcohol and aldehyde products and the numbers of the reactive intermediates on the catalyst surface leading to those products were quantified using transient kinetic analysis. The transient experiments were performed at various flowrates to evaluate the importance of product readsorption on the kinetic parameters. Transient kinetic analysis associated with PdRe/SiO_2 was performed over alcohol selectivity ranges from 64-80%.

The time constant of the gas-phase holdup in the reactor system was measured as the total flow rate was varied over the range of 15 cm^3 min^{-1} to 60 cm^3 min^{-1}. The gas-phase holdup could not be measured directly during the alcohol transient because the decay of the methane tracer was faster than the sampling rate. The very short time constant of the gas-phase holdup (measured

during aldehyde experiments) was negligible in comparison to the alcohol transient times and was not included in the calculation of the mean surface residence times for species leading to alcohols. In contrast, the mean surface residence times of species leading to aldehyde products was much shorter than those leading to alcohols, so the gas phase holdup was properly accounted for in the aldehyde transient results.

Examples of normalized transient curves during carboxylic acid reduction are shown in Figure 10. Since the reaction is zero order in acid, a slight difference in the gas phase concentrations of C_3 and C_4 acids will not affect their measured reaction rates. By integrating the response after the switch in reactant, the mean surface residence time of the species leading to a specified product was calculated. The mean surface residence times for reactants leading to alcohol products during the reduction of propionic and butyric acid are shown in Figure 11 as a function of inverse flowrate. An estimate of the intrinsic mean surface residence time in the absence of readsorption effects (τ_0) can be derived from extrapolating the lines in Figure 11 to infinite flowrate ($1/F = 0$). The intrinsic mean surface residence time is then used to determine an intrinsic turnover frequency and the number of reactive intermediates on the catalyst, N_i in the absence of readsorption effects. These results are summarized in Table 4.

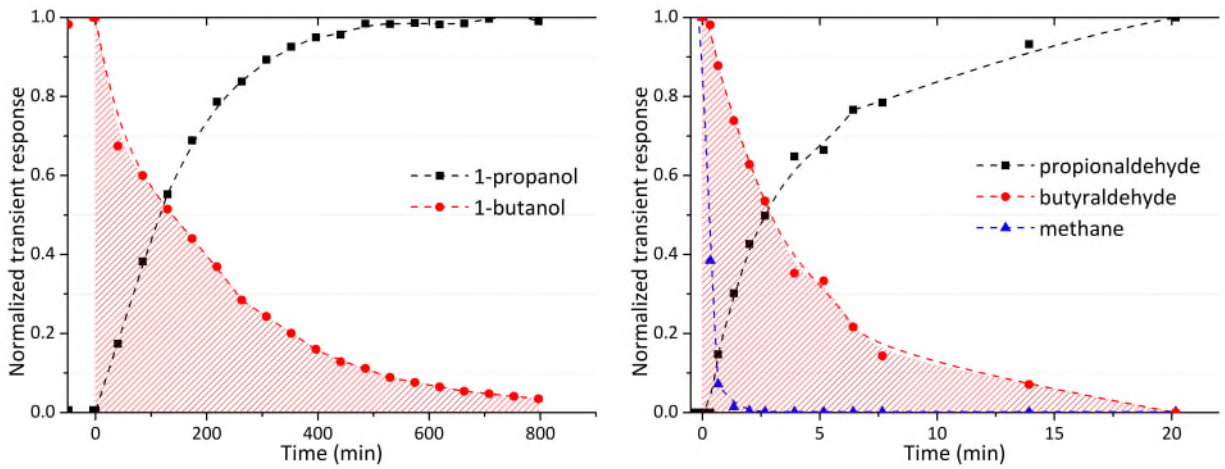

Figure 10: **Example of transient product responses during carboxylic acid reduction obtained after a reactant switch from butyric acid to propionic acid.**

Table 4: **Kinetic parameters derived from transient kinetic analysis of 1 kPa propionic and butyric acid reduction in 0.1 MPa H_2 at 433 K, including the ratio of reactive intermediates to Re atoms N_i/Re.**

Catalyst	Product	Rate of formation[a] (mol g_{cat}^{-1} h^{-1})	τ_0 (min)	TOF[b] (s^{-1})	N_i/Re[c]
$PdRe/SiO_2$	1-propanol	1.6×10^{-4}	81	2.1×10^{-4}	0.59
	propionaldehyde	6.3×10^{-5}	2.0	8.3×10^{-3}	0.006
	1-butanol	6.9×10^{-5}	130	1.3×10^{-4}	0.40
	butyraldehyde	3.1×10^{-5}	2.0	8.4×10^{-3}	0.003
Re/SiO_2	propionaldehyde	3.7×10^{-5}	1.4	1.1×10^{-2}	0.003
	butyraldehyde	2.1×10^{-5}	1.7	1.0×10^{-2}	0.002

(a) Calculated by extrapolation to infinite flowrate
(b) TOF is calculated as τ_0^{-1}
(c) Ratio of intermediates leading to specified product divided by total Re in sample

The intrinsic TOF for 1-propanol formation over $PdRe/SiO_2$ is 1.6 times that of 1-butanol formation, which is very similar to the ratio of the global rates of formation of 1-propanol to 1-

butanol of 2.3. Therefore, the same fraction of the active surface is involved in both reactions. The number of reactive surface intermediates leading to 1-propanol or 1-butanol is calculated to be 59% or 40% of the total Re in the $PdRe/SiO_2$ catalyst respectively, (see Table 4). Variation of the H_2 pressure during the transient experiment revealed a nearly first-order dependence on H_2 of the intrinsic TOF of alcohol formation from both butyric and propionic acids, as shown in Figure S10. The intrinsic kinetic parameters determined at 0.2 MPa (as summarized in Table S4 and Figure S11) are also consistent with approximately 50% of the Re participating in the reaction. A mean surface residence time of 450 min (corresponding to a 0.1 N_i/Re ratio) was observed for 1-propanol formation on Re/SiO_2 at 0.1 MPa H_2 pressure and 1 kPa propionic acid, but the effects of flowrate could not be eliminated due to limits on the detection of the very minor alcohol products. The intrinsic TOF for production of aldehydes on the $PdRe/SiO_2$ and Re/SiO_2 catalysts was about 2 orders of magnitude greater than that of alcohols formed over $PdRe/SiO_2$. All associated transient response results can be found in Tables S2 and S3 in the supporting information.

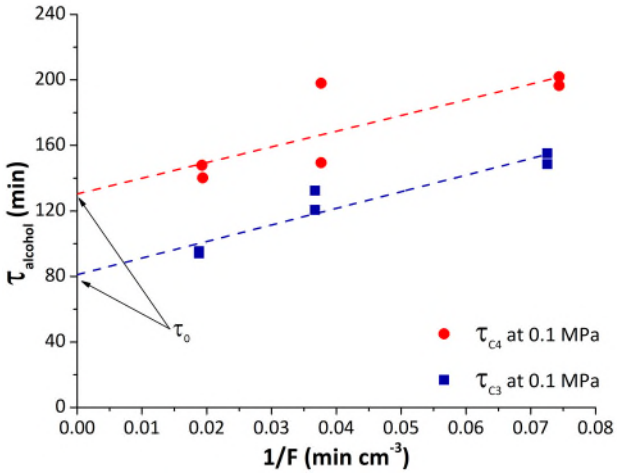

Figure 11: **Mean surface residence times of species leading to alcohols at 433 K over PdRe/SiO_2 extrapolated to infinite flowrate to remove artifacts from product readsorption. Red circles represent results from butyric acid conversion at 0.1 MPa H_2 pressure while blue squares represent results from propionic acid conversion at 0.1 MPa H_2 pressure. The conversion ranged from 2.5-7% over the range of flowrates used.**

DISCUSSION

Reducibility of PdRe/SiO_2

The results from H_2 TPR and *in-situ* XAS confirm that Pd facilitates the reduction of Re^{7+} on the air-exposed, as-synthesized Pd-promoted Re/SiO_2 catalyst at lower temperatures than required for the reduction of the un-promoted Re/SiO_2. This phenomenon is well established for Pt-promoted Re catalysts on Al_2O_3[41,61,62] and has been suggested previously using TPR in other supported Re systems promoted by Rh[63], Pd, Ru, and Ir.[30] The additional low-temperature reduction peak observed in H_2 TPR of the PdRe/SiO_2 catalyst compared to the Pd/SiO_2 catalyst (Figure 3) corresponds to the low-temperature partial reduction of Re^{7+} oxide likely by H_2 spillover. Results from H_2 chemisorption, which show that Re did not suppress formation of β-phase Pd hydride, suggest that some surface Pd in the PdRe sample is available for H_2 adsorption

and therefore for spillover to the Re. High-resolution STEM with EDS mapping also suggests that the metals on the PdRe catalyst remain highly dispersed during reaction, and that Re and Pd do not appear to form significant amounts of bimetallic nanoparticles. The Re appeared to be highly dispersed and Pd existed almost exclusively in larger well-dispersed metal particles, which is also consistent with extensive spillover of H from Pd as the main reason for enhanced Re reduction in the presence of Pd. The XAS performed in this work suggests that under reaction conditions, Pd in the $PdRe/SiO_2$ remains entirely metallic, while the Re resides in an average oxidation state of around 4+. Partially-reduced Re oxides have been reported to demonstrate carboxylic acid reduction activity, and Re^{4+} in particular has been observed to have remarkable selectivity to alcohols in the catalytic reduction of carboxylic acids to alcohols.[64] Analysis of the Re-O interatomic distances in the EXAFS is consistent with XANES, indicating the Re is partially reduced to around Re^{4+} from its initial Re^{7+} state. The Re-O first shell interatomic distance in the bimetallic PdRe sample is slightly longer than the interatomic distance of Re-O in the Re^{4+} standard, whether or not the sample was pretreated prior to reaction. Evidently, there was little contribution to the EXAFS from higher oxidation states and we conclude that nearly all of the Re in the bimetallic catalyst was partially reduced in the presence of Pd and H_2. Likewise, very little evidence from Re-Re scattering associated with zero-valent Re was observed on the $PdRe/SiO_2$ catalyst. For the monometallic Re catalyst, the as-synthesized sample revealed a short Re-O interatomic distance and XANES features consistent with Re^{7+} oxide species. High-temperature pretreatment in H_2 resulted in nearly complete reduction of Re to the metal. It should be emphasized that a high temperature pretreatment was required for an active Re/SiO_2 catalyst. Consistent with H_2 TPR, results from XANES and EXAFS showed negligible reduction of

Re/SiO_2 at 453 K. Evidently the predominant Re^{7+} species that is present after low temperature reduction is the least active Re species for carboxylic acid reduction in H_2 at 433 K.

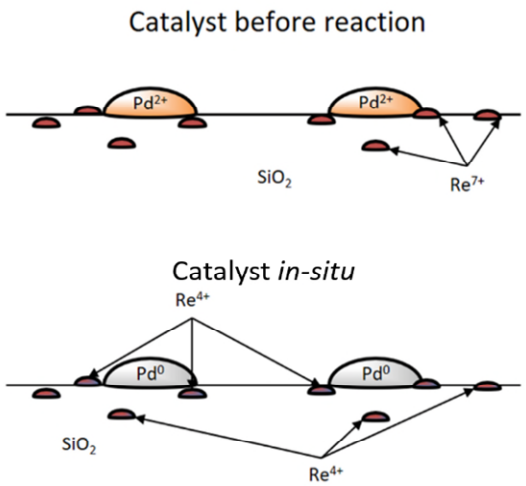

***Figure 12*: Representation of $PdRe/SiO_2$ catalyst surface before and after pretreatments leading to an active catalyst.**

Based on the interpretation of the XAS results, H_2 and CO chemisorption, H_2 TPR, and STEM-EDS, a schematic for the evolution of the catalyst structure is summarized in Figure 12. The metals in both the Re and PdRe catalysts are expected to be completely oxidized after catalyst synthesis. However, the chemical state of each catalyst under reaction conditions is related strongly to its treatment before reaction. Monometallic Re/SiO_2 was observed to remain in a highly oxidized state under reaction conditions, both without pretreatment and with pretreatment at 453 K under 4% H_2. When exposed to high-temperature pretreatment in H_2 at 673 K, the monometallic catalyst appeared to be nearly completely reduced. The Re in the $PdRe/SiO_2$ catalyst on the other hand was only partially reduced both with and without low-temperature pretreatments in H_2. Under gas phase conditions, controlled reduction of the Re to an intermediate oxidation state for reaction occurs mainly when the catalyst is promoted by Pd. Our results contrast those in which a

$PdRe/SiO_2$ catalyst was reported to contain a significant fraction of Re metal after liquid-phase reduction of stearic acid to stearyl alcohol[37], but are consistent with other works that propose partially reduced Re oxide with Re in about a 4+ oxidation state as the average oxidation state of Re species on the catalyst.

Surface Reactions

The transient kinetics experiments reveal the number of intermediates that ultimately form products, but there can be species that are equilibrated on the surface and actually convert in the reverse direction during the transient. Therefore, the number of reactive intermediates determined by this method is actually a lower bound on the number of active sites on the catalyst surface. Using transient kinetic analysis, the reported ratio of reactive intermediates that produce alcohols and aldehydes to Re atoms on the catalyst operating at steady state is about 50% in the $PdRe/SiO_2$ catalyst (Table 4). We have based our analysis on the ratio of intermediates to total Re atoms present. It is quite possible that some of the intermediates leading to product are located on the Pd surface. The reported uptake of H_2 in the $PdRe/SiO_2$ catalyst would correspond to a maximum dispersion of Pd of 60%, with the real value likely closer to that observed in the monometallic Pd/SiO_2 of 39%. Using a Pd dispersion of 60% as an upper bound, the ratio of surface Pd atoms to total Re on the catalyst is 1:7.5. Since the number of surface intermediates leading to alcohols and aldehydes far outnumbers the amount of potentially available Pd by about 3 to 1, we conclude that at least half of all the Re in the $PdRe/SiO_2$ catalyst participates in the reduction of these acids to alcohols under reaction conditions, whereas in the absence of Pd, a much smaller fraction of Re participates in the reaction. Since at least 50% of the Re in the $PdRe/SiO_2$ participates in the reaction, the results from *in-situ* XAS characterization should be relevant to identifying the active form of the Re.

Takeda et al.[36] reported a turnover frequency of 4.0 h^{-1} (or $1.1x10^{-3}$ s^{-1}) at 413 K under 8 MPa H_2 for stearic acid reduction in liquid dioxane solvent using an analogous $PdRe/SiO_2$ catalyst. Extrapolating the intrinsic TOF at 433 K for vapor phase propionic acid reduction to 1-propanol to 8 MPa H_2 (assuming first order in H_2) gives an estimated TOF of $1.7x10^{-2}$ s^{-1} on our $PdRe/SiO_2$, which is about an order of magnitude greater than that reported by Takeda et al. Our higher estimated TOF can be explained by several factors. First, Takeda et al. normalize their observed rate by the total amount of Re in their catalyst, whereas our TOF from transient kinetic studies involves only half of the Re in our sample. Second, the reaction in the current work was studied at a temperature 20 K higher than that used by Takeda et al. Finally, influences of chain length and solvent might affect the reaction rate between the two systems.

The fraction of Re in $PdRe/SiO_2$ associated with aldehyde formation was two orders of magnitude smaller than that associated with alcohol formation but turned over much more rapidly. A slightly smaller number of aldehyde-producing sites having the same turnover frequency was also observed on the monometallic Re/SiO_2. Based on the observed trends in reactivity, the Re oxidation state appears to play a role in the selectivity of carboxylic acid reduction to alcohol or aldehyde products. Promotion of the Re with Pd appears to be responsible for the enhanced reduction of Re to a more active, partially reduced form. The presence of Pd may also increase the hydrogen availability to the active intermediate Re oxides, thereby hydrogenating aldehydes to alcohols. The importance of the distance between Re and Pd for spillover to take place is evidenced by the results from the physical mixture of Pd/SiO_2 and Re/SiO_2. When the two metals were separated on different support particles, the mixed catalyst bed was still able to reduce propionic acid to a majority of 1-propanol, albeit at 30% the rate of the two metals on the same support particles. This result demonstrates that Pd is capable of promoting the Re for selective reduction

of carboxylic acids to alcohols, even when not in direct physical contact with the Re. The first order dependence of the turnover frequency on the dihydrogen pressure indicates that hydrogen availability is critical to the activity of the Re-based catalysts studied here. Transient kinetic analysis suggests that changing the dihydrogen pressure from 0.1 to 0.2 MPa did not increase the number of reactive intermediates on the surface. The higher H_2 pressure may instead facilitate a more rapid hydrogenation of adsorbed intermediates leading to alcohols.

CONCLUSIONS

Results from extensive characterization of the monometallic Pd and Re catalysts as well as the bimetallic PdRe catalyst revealed the structural evolution of the active $PdRe/SiO_2$ catalyst for the reduction of propionic acid to 1-propanol. During reducing pretreatment or reaction, the highly dispersed Re (7+) oxide is partially reduced to a Re (~4+) oxide, through a process that is facilitated by the presence of metallic Pd, presumably via hydrogen spillover. This intermediate oxide of Re is a catalytically active phase of Re since metallic Pd does not convert carboxylic acids under the conditions of study. Transient kinetic experiments revealed at least 50% of the Re is involved in the catalytic turnover. The importance of the transient kinetic experiments, which have not previously been performed on this catalytic system, cannot be understated since the results indicate the active catalytic sites are not a minority species or associated with defects, but instead are associated with at least half of the Re in the sample. Therefore, results from X-ray absorption spectroscopy, which are associated with the average of all Re species present during the interrogation, are directly relevant to catalysis.

Corresponding Author

*Robert J. Davis

E-mail: rjd4f@virginia.edu

Phone: 1 (434)-924-6284

Funding Sources

This material is based upon work supported by the National Science Foundation (NSF) under Award No. EEC-0813570. Any opinions, findings, and conclusions or recommendations expressed in this material are those of the author(s) and do not necessarily reflect the views of the NSF.

Notes

The authors declare no competing financial interest.

Acknowledgements

Electron microscopy was performed in the University of Virginia's Nanomaterials Characterization Facility, and at Oak Ridge National Laboratory's Center for Nanophase Materials Science.

This work was carried out with the support of the Diamond Light Source on proposal number SP13561-1. We thank Diamond Light Source for access to beamline B18 that contributed to the results presented here. Dr. Giannantonio Cibin is also acknowledged for his assistance in the setup of the *in-situ* reactor at Diamond Light Source. This research also used beamline 8-ID of the National Synchrotron Light Source II, a U.S. Department of Energy (DOE) Office of Science User Facility operated for the DOE Office of Science by Brookhaven National Laboratory under Contract No. DE-SC0012704.

Supporting Information

STEM-HAADF with EDS elemental mapping, fitting results for EXAFS standards collected at the Re L_{III}-edge and Pd K-edge, XANES collected at the Pd K-edge, evidence for differential conversion in the reduction of propionic and butyric acid, mean surface residence times collected during reactant switches between butyric acid and propionic acid.

References

(1) Corma, A.; Iborra, S.; Velty, A. Chemical Routes for the Transformation of Biomass into Chemicals. *Chem. Rev.* **2007**, *107* (6), 2411–2502, DOI 10.1021/cr050989d.

(2) Bozell, J. J.; Petersen, G. R. Technology Development for the Production of Biobased Products from Biorefinery Carbohydrates -- the US Department of Energy's "Top 10" Revisited. *Green Chem.* **2010**, *12* (4), 539, DOI 10.1039/b922014c.

(3) Chheda, J. N.; Huber, G. W.; Dumesic, J. A. Liquid-Phase Catalytic Processing of Biomass-Derived Oxygenated Hydrocarbons to Fuels and Chemicals. *Angew. Chem. Int. Ed. Engl.* **2007**, *46* (38), 7164–7183, DOI 10.1002/anie.200604274.

(4) Besson, M.; Gallezot, P.; Pinel, C. Conversion of Biomass into Chemicals over Metal Catalysts. *Chem. Rev.* **2014**, *114* (3), 1827–1870, DOI 10.1021/cr4002269.

(5) Vennestrøm, P. N. R.; Osmundsen, C. M.; Christensen, C. H.; Taarning, E. Beyond Petrochemicals: The Renewable Chemicals Industry. *Angew. Chemie - Int. Ed.* **2011**, *50* (45), 10502–10509, DOI 10.1002/anie.201102117.

(6) Schlaf, M. Selective Deoxygenation of Sugar Polyols to α,ω-Diols and Other Oxygen Content Reduced Materials--a New Challenge to Homogeneous Ionic Hydrogenation and

Hydrogenolysis Catalysis. *Dalton Trans.* **2006**, No. 39, 4645–4653, DOI 10.1039/b608007c.

(7) Gervajio, G. C. Fatty Acids and Derivatives from Coconut Oil. In *Kirk-Othmer Encyclopedia of Chemical Technology*; 2012; pp 1–38.

(8) Gallezot, P. Conversion of Biomass to Selected Chemical Products. *Chem. Soc. Rev.* **2012**, *41* (4), 1538–1558, DOI 10.1039/c1cs15147a.

(9) Chen, Y.; Chang, C. Cu-B_2O_3/SiO_2, an Effective Catalyst for Synthesis of Fatty Alcohol from Hydrogenolysis of Fatty Acid Esters. *Catal. Letters* **1997**, *48*, 2–5, DOI 10.1023/A:1019010600765.

(10) Nebesh, E.; Kelly, D. G.; Novak, L. T. Copper Chromite Catalyst and Process for Preparation Said Catalyst. US5124295A, 1992.

(11) Thakur, D. S.; Carrick, W. J. Copper Chromite Hydrogenation Catalysts for Production of Fatty Alcohols. US20120136179A1, 2012.

(12) Huang, H.; Wang, S.; Wang, S.; Cao, G. Deactivation Mechanism of Cu/Zn Catalyst Poisoned by Organic Chlorides in Hydrogenation of Fatty Methyl Ester to Fatty Alcohol. *Catal. Letters* **2009**, *134* (3–4), 351–357, DOI 10.1007/s10562-009-0247-x.

(13) Brands, D. S.; UA-Sai, G.; Poels, E. K.; Bliek, A. Sulfur Deactivation of Fatty Ester Hydrogenolysis Catalysts. *J. Catal.* **1999**, *186* (1), 169–180, DOI 10.1006/jcat.1999.2553.

(14) Wu, H.; Karanjikar, M.; San, K.-Y. Metabolic Engineering of Escherichia Coli for Efficient Free Fatty Acid Production from Glycerol. *Metab. Eng.* **2014**, *25*, 82–91, DOI 10.1016/j.ymben.2014.06.009.

(15) Jansen, M. L. A.; van Gulik, W. M. Towards Large Scale Fermentative Production of Succinic Acid. *Curr. Opin. Biotechnol.* **2014**, *30*, 190–197, DOI 10.1016/j.copbio.2014.07.003.

(16) Czernik, S.; Bridgwater, A. V. Overview of Applications of Biomass Fast Pyrolysis Oil. *Energy and Fuels* **2004**, *18* (2), 590–598, DOI 10.1021/ef034067u.

(17) Primo, A.; Concepción, P.; Corma, A. Synergy between the Metal Nanoparticles and the Support for the Hydrogenation of Functionalized Carboxylic Acids to Diols on Ru/TiO_2. *Chem. Commun.* **2011**, *47* (12), 3613, DOI 10.1039/c0cc05206j.

(18) Rachmady, W.; Vannice, M. Acetic Acid Hydrogenation over Supported Platinum Catalysts. *J. Catal.* **2000**, *192* (2), 322–334, DOI 10.1006/jcat.2000.2863.

(19) Toba, M.; Tanaka, S.; Niwa, S.; Mizukami, F.; Koppány, Z.; Guczi, L.; Cheah, K.-Y.; Tang, T.-S. Synthesis of Alcohols and Diols by Hydrogenation of Carboxylic Acids and Esters over Ru–Sn–Al_2O_3 Catalysts. *Appl. Catal. A Gen.* **1999**, *189* (2), 243–250, DOI 10.1016/S0926-860X(99)00281-1.

(20) Chen, L.; Li, Y.; Zhang, X.; Zhang, Q.; Wang, T.; Ma, L. Mechanistic Insights into the Effects of Support on the Reaction Pathway for Aqueous-Phase Hydrogenation of Carboxylic Acid over the Supported Ru Catalysts. *Appl. Catal. A Gen.* **2014**, *478*, 117–128, DOI 10.1016/j.apcata.2014.03.038.

(21) Pritchard, J.; Filonenko, G. A.; van Putten, R.; Hensen, E. J. M.; Pidko, E. A. Heterogeneous and Homogeneous Catalysis for the Hydrogenation of Carboxylic Acid Derivatives: History, Advances and Future Directions. *Chem. Soc. Rev.* **2015**, *44*, 3808–

3833, DOI 10.1039/C5CS00038F.

(22) Broadbent, H. S.; Bartley, W. J. Rhenium Catalysts. VII. Rhenium(VI) Oxide. *J. Org. Chem.* **1963**, *28* (9), 2345–2347, DOI 10.1021/jo01044a046.

(23) Broadbent, H. S.; Seegmiller, D. W. Rhenium Catalysts. VIII. Rhenium(II) Oxide Dihydrate from Perrhenate via Alkali Metal-Amine Reductions. *J. Org. Chem.* **1963**, *28* (9), 2347–2350, DOI 10.1021/jo01044a047.

(24) Broadbent, H. S.; Campbell, G. C.; Bartley, W. J.; Johnson, J. H. Rhenium and Its Compounds as Hydrogenation Catalysts. III. Rhenium Heptoxide. *J. Org. Chem.* **1959**, *24* (12), 1847–1854, DOI 10.1021/jo01094a003.

(25) Broadbent, H. S.; Johnson, J. H. Rhenium Catalysts. IV. Rhenium(III) Oxide from Perrhenate via Borohydride Reduction. *J. Org. Chem.* **1962**, *27* (12), 4400–4402, DOI 10.1021/jo01059a065.

(26) Snappe, R.; Bouronville, J.-P. Procedure for Producing Alcohols via Catalytic Hydrogenation of Esters of Organic Acids. FR2505819A1, 1981.

(27) Mabry, M.; Prichard, W.; Ziemecki, S. Process for Making Tetrahydrofuran and 1, 4-Butanediol Using Pd/Re Hydrogenation Catalyst. US4550185A, 1985.

(28) Rao, V. Process for Preparing Butyrolactones and Butanediols. US4782167A, 1988.

(29) Kitson, M.; Williams, P. S. Catalyzed Hydrogenation of Carboxylic Acids and Their Anhydrides to Alcohols and/or Esters. US4985572A, 1991.

(30) Takeda, Y.; Nakagawa, Y.; Tomishige, K. Selective Hydrogenation of Higher Saturated

Carboxylic Acids to Alcohols Using a ReO_x–Pd/SiO_2 Catalyst. *Catal. Sci. Technol.* **2012**, *2* (11), 2221, DOI 10.1039/c2cy20302b.

(31) Corbel-Demailly, L.; Ly, B.-K.; Minh, D.-P.; Tapin, B.; Especel, C.; Epron, F.; Cabiac, A.; Guillon, E.; Besson, M.; Pinel, C. Heterogeneous Catalytic Hydrogenation of Biobased Levulinic and Succinic Acids in Aqueous Solutions. *ChemSusChem* **2013**, *6* (12), 2388–2395, DOI 10.1002/cssc.201300608.

(32) Rozmysłowicz, B.; Kirilin, A.; Aho, A.; Manyar, H.; Hardacre, C.; Wärnå, J.; Salmi, T.; Murzin, D. Y. Selective Hydrogenation of Fatty Acids to Alcohols over Highly Dispersed ReO_x/TiO_2 Catalyst. *J. Catal.* **2015**, *328*, 197–207, DOI 10.1016/j.jcat.2015.01.003.

(33) Minh, D. P.; Besson, M.; Pinel, C.; Fuertes, P.; Petitjean, C. Aqueous-Phase Hydrogenation of Biomass-Based Succinic Acid to 1,4-Butanediol Over Supported Bimetallic Catalysts. *Top. Catal.* **2010**, *53* (15–18), 1270–1273, DOI 10.1007/s11244-010-9580-y.

(34) Tapin, B.; Epron, F.; Especel, C.; Ly, B. K.; Pinel, C.; Besson, M. Influence of the Re Introduction Method onto Pd/TiO_2 Catalysts for the Selective Hydrogenation of Succinic Acid in Aqueous-Phase. *Catal. Today* **2014**, *235*, 127–133, DOI 10.1016/j.cattod.2014.02.018.

(35) Ly, B. K.; Minh, D. P.; Pinel, C.; Besson, M.; Tapin, B.; Epron, F.; Especel, C. Effect of Addition Mode of Re in Bimetallic Pd–Re/TiO_2 Catalysts Upon the Selective Aqueous-Phase Hydrogenation of Succinic Acid to 1,4-Butanediol. *Top. Catal.* **2012**, *55* (7–10), 466–473, DOI 10.1007/s11244-012-9813-3.

(36) Ly, B. K.; Tapin, B.; Aouine, M.; Delichere, P.; Epron, F.; Pinel, C.; Especel, C.; Besson, M. Insights into the Oxidation State and Location of Rhenium in Re-Pd/TiO_2 Catalysts for Aqueous-Phase Selective Hydrogenation of Succinic Acid to 1,4-Butanediol as a Function of Palladium and Rhenium Deposition Methods. *ChemCatChem* **2015**, *7* (14), 2161–2178, DOI 10.1002/cctc.201500197.

(37) Takeda, Y.; Tamura, M.; Nakagawa, Y.; Okumura, K.; Tomishige, K. Characterization of Re-Pd/SiO_2 Catalysts for Hydrogenation of Stearic Acid. *ACS Catal.* **2015**, *5* (11), 7034–7047, DOI 10.1021/acscatal.5b01054.

(38) Dent, A. J.; Cibin, G.; Ramos, S.; Smith, A. D.; Scott, S. M.; Varandas, L.; Pearson, M. R.; Krumpa, N. A.; Jones, C. P.; Robbins, P. E. B18: A Core XAS Spectroscopy Beamline for Diamond. *J. Phys. Conf. Ser.* **2009**, *190* (1), DOI 10.1088/1742-6596/190/1/012039.

(39) Palomino, R. M.; Stavitski, E.; Waluyo, I.; Chen-Wiegart, Y. chen K.; Abeykoon, M.; Sadowski, J. T.; Rodriguez, J. A.; Frenkel, A. I.; Senanayake, S. D. New In-Situ and Operando Facilities for Catalysis Science at NSLS-II: The Deployment of Real-Time, Chemical, and Structure-Sensitive X-Ray Probes. *Synchrotron Radiat. News* **2017**, *30* (2), 30–37, DOI 10.1080/08940886.2017.1289805.

(40) Ravel, B.; Newville, M. ATHENA, ARTEMIS, HEPHAESTUS: Data Analysis for X-Ray Absorption Spectroscopy Using IFEFFIT. *J. Synchrotron Radiat.* **2005**, *12* (4), 537–541, DOI 10.1107/S0909049505012719.

(41) Hilbrig, F.; Michel, C.; Haller, G. L. A XANES-TPR Study of PtRe/Al_2O_3 Catalysts. *J. Phys. Chem.* **1992**, *96* (24), 9893–9899, DOI 10.1021/j100203a058.

(42) Tougerti, A.; Cristol, S.; Berrier, E.; Briois, V.; La Fontaine, C.; Villain, F.; Joly, Y. XANES Study of Rhenium Oxide Compounds at the L 1 and L 3 Absorption Edges. *Phys. Rev. B - Condens. Matter Mater. Phys.* **2012**, *85* (12), 1–8, DOI 10.1103/PhysRevB.85.125136.

(43) Shannon, S.; Goodwin, J. Characterization of Catalytic Surfaces by Isotopic-Transient Kinetics during Steady-State Reaction. *Chem. Soc. Rev.* **1995**, 677–695, DOI 10.1021/cr00035a011.

(44) McClaine, B. C.; Davis, R. J. Importance of Product Readsorption during Isotopic Transient Analysis of Ammonia Synthesis on Ba-Promoted Ru/BaX Catalyst. *J. Catal.* **2002**, *211* (2), 379–386, DOI 10.1016/S0021-9517(02)93757-7.

(45) McClaine, B. C.; Davis, R. J. Isotopic Transient Kinetic Analysis of Cs-Promoted Ru/MgO during Ammonia Synthesis. *J. Catal.* **2002**, *210* (2), 387–396, DOI 10.1006/jcat.2002.3688.

(46) Calla, J. T.; Bore, M. T.; Datye, A. K.; Davis, R. J. Effect of Alumina and Titania on the Oxidation of CO over Au Nanoparticles Evaluated by ^{13}C Isotopic Transient Analysis. *J. Catal.* **2006**, *238* (2), 458–467, DOI 10.1016/j.jcat.2006.01.009.

(47) Calla, J. T.; Davis, R. J. Oxygen-Exchange Reactions during CO Oxidation over Titania- and Alumina-Supported Au Nanoparticles. *J. Catal.* **2006**, *241* (2), 407–416, DOI 10.1016/j.jcat.2006.05.017.

(48) Shou, H.; Davis, R. J. Multi-Product Steady-State Isotopic Transient Kinetic Analysis of CO Hydrogenation over Supported Molybdenum Carbide. *J. Catal.* **2013**, *306*, 91–99,

DOI 10.1016/j.jcat.2013.06.009.

(49) Birky, T. W.; Kozlowski, J. T.; Davis, R. J. Isotopic Transient Analysis of the Ethanol Coupling Reaction over Magnesia. *J. Catal.* **2013**, *298*, 130–137, DOI 10.1016/j.jcat.2012.11.014.

(50) Hanspal, S.; Young, Z. D.; Shou, H.; Davis, R. J. Multiproduct Steady-State Isotopic Transient Kinetic Analysis of the Ethanol Coupling Reaction over Hydroxyapatite and Magnesia. *ACS Catal.* **2015**, *5* (3), 1737–1746, DOI 10.1021/cs502023g.

(51) Pinna, F.; Signoretto, M.; Strukul, G.; Polizzi, S.; Pernicone, N. Pd-SiO2 Catalysts. Stability of β-PdHx as a Function of Pd Dispersion. *React. Kinet. Catal. Lett.* **1997**, *60* (1), 9–13, DOI 10.1007/BF02477683.

(52) Joyal, C. L. M.; Butt, J. B. Chemisorption and Disproportionation of Carbon Monoxide on Palladium/Silica Catalysts of Differing Percentage Metal Exposed. *J. Chem. Soc. Faraday Trans. 1* **1987**, *83* (9), 2757–2764, DOI 10.1039/f19878302757.

(53) Chądzyński, G. W.; Kubicka, H. Chemisorption of Hydrogen and Oxygen on γ-Alumina-Supported Rhenium. Part 1. Chemisorption of Hydrogen. *Thermochim. Acta* **1990**, *158* (2), 369–383, DOI 10.1016/0040-6031(90)80084-C.

(54) Thompson, S. T.; Lamb, H. H. Palladium-Rhenium Catalysts for Selective Hydrogenation of Furfural: Evidence for an Optimum Surface Composition. *ACS Catal.* **2016**, *6* (11), 7438–7447, DOI 10.1021/acscatal.6b01398.

(55) Nacheff, M. S.; Kraus, L. S.; Ichikawa, M.; Huffman, B. M.; Butt, J. B.; Sachtler, W. M. H. Characterization and Catalytic Function of Re^0 and Re^{4+} in $ReAl_2O_3$ and PtRe Al_2O_3

Catalysts. *J. Catal.* **1987**, *106* (1), 263–272, DOI 10.1016/0021-9517(87)90230-2.

(56) Kunkes, E. L.; Simonetti, D. A.; Dumesic, J. A.; Pyrz, W. D.; Murillo, L. E.; Chen, J. G.; Buttrey, D. J. The Role of Rhenium in the Conversion of Glycerol to Synthesis Gas over Carbon Supported Platinum-Rhenium Catalysts. *J. Catal.* **2008**, *260* (1), 164–177, DOI 10.1016/j.jcat.2008.09.027.

(57) Ziemecki, S. B.; Jones, G. A.; Michel, J. B. Surface Mobility of Re_2O_7 in the System $Re^{7+}Pd^0$ γ-Al_2O_3. *J. Catal.* **1986**, *99* (1), 207–217, DOI 10.1016/0021-9517(86)90213-7.

(58) Wang, C.; Cai, Y.; Wachs, I. E. Reaction-Induced Spreading of Metal Oxides onto Surfaces of Oxide Supports during Alcohol Oxidation : Phenomenon , Nature , and Mechanisms. *Langmuir* **1999**, *15* (4), 1223–1235, DOI 10.1021/la9807210.

(59) Krebs, B.; Müller, A.; Beyer, H. H. The Crystal Structure of Rhenium(VII) Oxide. *Inorg. Chem.* **1969**, *8* (3), 436–443, DOI 10.1021/ic50073a006.

(60) Jentys, A. Estimation of Mean Size and Shape of Small Metal Particles by EXAFS. *Phys. Chem. Chem. Phys.* **1999**, *1* (17), 4059–4063, DOI 10.1039/a904654b.

(61) Bolivar, C.; Charcosset, H.; Frety, R.; Primet, M.; Tournayan, L.; Betizeau, C.; Leclercq, G.; Maurel, R. Platinum-Rhenium/Alumina Catalysts I. Investigation of Reduction by Hydrogen. *J. Catal.* **1975**, *39* (2), 249–259, DOI 10.1016/0021-9517(75)90329-2.

(62) Mieville, R. L. Platinum-Rhenium Interaction: A Temperature-Programmed Reduction Study. *J. Catal.* **1984**, *87* (2), 437–442, DOI 10.1016/0021-9517(84)90203-3.

(63) Chia, M.; Pagán-Torres, Y. J.; Hibbitts, D.; Tan, Q.; Pham, H. N.; Datye, A. K.; Neurock, M.; Davis, R. J.; Dumesic, J. A. Selective Hydrogenolysis of Polyols and Cyclic Ethers

over Bifunctional Surface Sites on Rhodium-Rhenium Catalysts. *J. Am. Chem. Soc.* **2011**, *133* (32), 12675–12689, DOI 10.1021/ja2038358.

(64) Broadbent, H. S.; Selin, T. G. Rhenium Catalysts. VI. Rhenium(IV) Oxide Hydrate. *J. Org. Chem.* **1963**, *28* (9), 2343–2345, DOI 10.1021/jo01044a045.

GRAPHICAL ABSTRACT

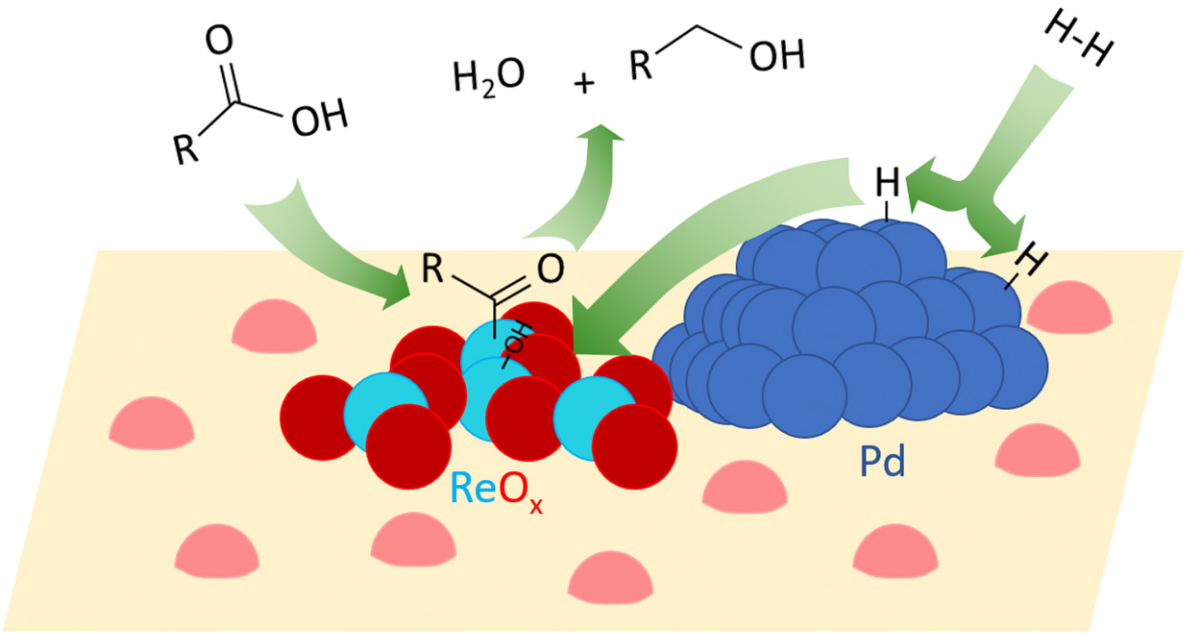

Synopsis: This study uses *in-situ* X-ray absorption spectroscopy and transient kinetic analysis to elucidate structure-performance relationships for a Pd-promoted ReO_x catalyst used in the reduction of carboxylic acids that can be derived from renewable biomass.